JOURNAL OF GEOPHYSICAL RESEARCH, VOL. 97, NO. C7, PAGES 11,357–11,371, JULY 15, 1992

Edge Waves in the Presence of Strong Longshore Currents

PETER A. HOWD[1]

College of Oceanography, Oregon State University, Corvallis

ANTHONY J. BOWEN

Department of Oceanography, Dalhousie University, Halifax, Nova Scotia, Canada

ROBERT A. HOLMAN

College of Oceanography, Oregon State University, Corvallis

A form of the linear, inviscid shallow water wave equation which includes alongshore uniform, but cross-shore variable, longshore currents and bathymetry is presented. This formulation provides a continuum between gravity waves (either leaky or edge waves) on a longshore current, and the recently discovered shear waves. In this paper we will concentrate on gravity wave solutions for which $V(x)/c < 1$, where $V(x)$ is the longshore current, and c is the edge wave celerity. The effects of the current can be uniquely accounted for in terms of a modification to the true beach profile, $h'(x) = h(x)[1 - V(x)/c]^{-2}$, where $h(x)$ is the true profile and $h'(x)$ is the effective profile. This is particularly useful in conceptualizing the combined effects of longshore currents and variable bottom topography. We have solved numerically for the dispersion relationship and the cross-shore shapes of edge waves on a plane beach under a range of current conditions. Changes to the edge wave alongshore wavenumber, κ, of over 50% are found for reasonable current profiles, showing that the departure from plane beach dispersion due to longshore currents can be of the same order as the effect of introducing nonplanar topography. These changes are not symmetric as they are for profile changes; $|\kappa|$ increases for edge waves opposing the current flow (a shallower effective profile), but decreases for those coincident with the flow (a deeper effective profile). The cross-shore structure of the edge waves is also strongly modified. As $|\kappa|$ increases (decreases), the nodal structure shifts landward (seaward) from the positions found on the test beach in the absence of a current. In addition, the predicted variances away from the nodes, particularly for the alongshore component of edge wave orbital velocity, may change dramatically from the no-current case. Many of the edge wave responses are related to the ratio V_{max}/c, where V_{max} is the maximum current, and to the dimensionless cross-shore scale of the current, $|\kappa|x(V_{max})$, where $x(V_{max})$ is the cross-shore distance to V_{max}. This is most easily understood in terms of the effective profile and the strong dependence of the edge waves on the details of the inner part of the beach profile. Inclusion of the longshore current also has implications regarding the role of edge waves in the generation of nearshore morphology. For example, in the absence of a current, two phase-locked edge waves of equal frequency and mode progressing in opposite directions are expected to produce a crescentic bar. However, in the presence of a current, the wavenumbers would differ, stretching the expected crescentic bar into a welded bar. A more interesting effect is the possibility that modifications to the edge waves due to the presence of a virtual bar in the effective profile could lead to the development of a real sand bar on the true profile. These modifications appear to be only weakly sensitive to frequency, in contrast to the relatively strong dependence of the traditional model of sand bar generation at infragravity wave nodes.

INTRODUCTION

Numerous authors have proposed that edge waves play an important role in a number of nearshore processes, including mean circulation patterns [*Bowen and Inman*, 1969], the generation of nearshore morphology [*Holman and Bowen*, 1982], and momentum and energy transfer [*Elgar and Guza*, 1985]. Studies have shown that the shoreline expression of wave energy, the swash, can be dominated by infragravity motions with up to 70% of the variance of the incident gravity waves offshore [*Guza and Thornton*, 1982; *Holman and Sallenger*, 1985]. They are also an energetic part of the wave spectrum in the surf zone [*Holman*, 1981; *Guza and Thornton*, 1985; *Howd et al.*, 1991*a*].

Much of the interest in edge waves arises from the observation that their length scales are similar to those of sand bar systems, both in the cross shore [*Short*, 1975; *Bowen*, 1981] and in the alongshore for three-dimensional systems [*Bowen and Inman*, 1971; *Holman and Bowen*, 1982]. In all these cases, the sand bars are hypothesized to result from the nodal structure of the infragravity wave drift velocities. Unlike reflected incident wind waves, which have nodes every 10–20 m in the cross shore, infragravity wave nodes are typically spaced at 50- to 100-m intervals, closely matching the observed scales of sand bars.

The description of edge wave dynamics on beaches began with the consideration of two analytically tractable cases, the plane sloping profile $h(x) = \beta x$, [*Eckart*, 1951] and the exponential profile $h(x) = h_0(1 - e^{-\alpha x})$ [*Ball*, 1967]. *Holman and Bowen* [1979] and *Kirby et al.* [1981] used

[1]Now at Center for Coastal Geology, U.S. Geological Survey, St. Petersburg, Florida.

Paper number 92JC00858.
0148-0227/92/92JC-00858$05.00

numerical models to predict the dispersion relation and cross-shore shape of edge waves on irregular and barred topography, respectively. *Holman and Bowen* [1979] showed that assuming a profile shape for which an analytic result exists may lead to errors of up to 100% in κ for predictions of the dispersion relation. Numerical solutions in both studies show two related kinematic effects, the relative change of edge wave amplitudes away from the shoreline (compared with the plane beach case) and the associated movement of the nodal structure. *Kirby et al.* [1981] found that over a limited frequency range, distortion of edge wave shapes occurred such that elevation antinodes were attracted to the cross-shore location of a bar crest. The complexity of these numerical approaches is great, however, and many later researchers have simply assumed one of the analytic forms of the beach profile to be adequate [*Holman and Bowen*, 1984; *Sallenger et al.*, 1985; *Howd et al.*, 1991*a*].

Kenyon [1972] considered the influence of longshore currents on edge waves, analytically modeling the case of a plane beach with a longshore current constantly increasing in the offshore direction ($V(x) = \vartheta_1 x$). He found systematic variations in edge wave dispersion, although his theory was only valid for a current, $V(x)$, that remained very small compared with the celerity of the edge wave. While this approximation may hold for shelf-scale phenomena, it is routinely violated in the nearshore, both in terms of the constant shear and the magnitude of $V(x)$ relative to the edge wave celerity.

To test hypotheses regarding the generation of edge waves (for instance, *Gallagher* [1971]) and to correctly interpret measurements made in the field, the dispersion relationship and the cross-shore structure of the edge waves must be well understood. Because many measurements are made in the surf zone, and the data transformed to predict the shoreline amplitudes of the edge waves, it is important that the cross-shore shape of the edge waves be accurately predicted. It is necessary to determine not only the edge wave mode through the dispersion relationship, but also to relate the variance at any cross-shore location to the reference value at the shoreline. It will be shown that incorporation of both bathymetric and current effects are required for this task.

In the next section we will explore the role of the cross-shore structure of the mean longshore current, $V(x)$, in modifying edge waves in the nearshore. A conceptual framework for understanding the longshore current effects is followed by the derivation of the governing equations for low-frequency waves in the presence of irregular topography $h(x)$ and longshore current $V(x)$. While the equation is valid for all low-frequency motions where the Coriolis effect is not important (edge waves, leaky waves, and the recently discovered shear waves), we will concentrate for the remainder of this paper on edge waves. Results from a series of synthetic tests designed to examine the role currents play in modifying edge wave properties will be presented. Implications of these effects are then discussed. The improvements in describing edge wave dispersion and the changes in the cross-shore variance structure resulting from the inclusion of longshore currents are shown using data collected during a large field experiment. Finally, we will present a new hypothesis for the generation of sand bars based on changes in sediment transport resulting from edge wave modification by a strong longshore current.

THEORY

The nearshore, where shallow water wave celerities are a function of the water depth, $\sqrt{gh}$, has the possibility of trapping wave motions through refraction offshore and reflection at the shoreline (where the depth goes to zero). This behavior can be viewed as a waveguide, in direct analogy to other geophysical waveguides. The discrete set of resonant motions trapped in the nearshore waveguide are called edge waves, while leaky waves are those free waves which, upon reflection from the shoreline, escape the nearshore waveguide to deep water. A critical value of the alongshore radial wavenumber, $\kappa = 2\pi/L_y$, of the motion separates the two regimes. The sign of κ determines the direction of wave progression. (Throughout this paper the radial measures for wavenumber and frequency will be represented by κ and $\sigma = 2\pi/T$, and the cyclic measures by $k = 1/L_y$ and $f = 1/T$, where L_y is the alongshore wavelength and T is the wave period).

Two major modifications to the properties of the nearshore waveguide are sand bars and longshore currents (Figure 1). A comparison of their refractive effects is instructive. Sand bars modify the waveguide by changing the water depth. The sand bar crest, a depth minimum, is the location of a local celerity minimum and provides a focusing of wave rays at that location. A bar trough, meanwhile, is a local celerity maximum and leads to divergence of wave rays. While topography may be generally expected to change the cross-shore structure and wavenumber of an edge wave, the changes should be symmetric for waves progressing either direction along the coast.

A longshore current modifies the waveguide in a similar manner. Edge waves travelling into the current experience refractive focusing of the wave rays at the cross-shore location of the maximum longshore current, the location where opposition to their progression is the greatest. This response is similar to what we expect for the case of the sand bar discussed above. In contrast, the wave rays of edge waves traveling with the current diverge at the longshore current maximum, mimicking behavior that would be expected over a local depth maximum (trough topography). Edge waves of equivalent mode and frequency traveling in opposite directions on a beach with a longshore current will be modified differently.

General changes in the dispersion relationship due to longshore currents can be predicted. We expect that edge waves traveling into (with) a current will propagate slower (faster) and have larger (smaller) $|\kappa|$ values than those on the same beach in the absence of a longshore current. The current acts to either decrease (for edge waves traveling into the current) or increase (edge waves traveling with the current) the observed alongshore phase speed. To summarize, we expect there to be a relationship between longshore currents and apparent modifications to the beach profile seen by the edge waves. These changes are no longer the same for both directions of edge wave progression, introducing asymmetry to the problem.

This conceptual treatment of the nearshore as a waveguide can be formalized in a theoretical description of edge wave behavior by inclusion of variable topography and longshore

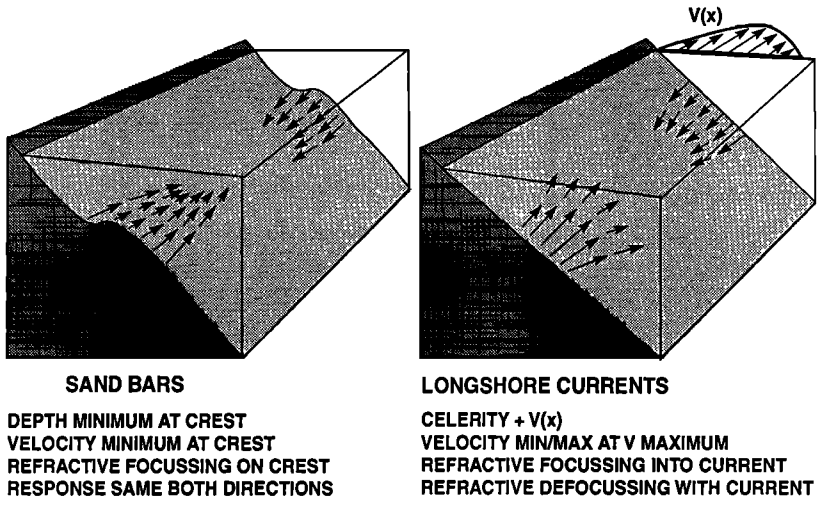

Fig. 1. Modification to the nearshore waveguide modification by the presence of a longshore current is analogous to that of bar and trough topography. The edge wave response to a sand bar is independent of the direction of edge wave propagation; wave rays refract and focus on the crest and diverge in the deeper trough. In the case of the longshore current on a plane beach, the effects are opposite for the different directions of edge wave propagation. Edge wave rays progressing into the current are refracted to focus on the current maximum (as if it were a bar), while those progressing with the current diverge as if they were in the trough of a bar.

currents in the inviscid shallow water equations for conservation of momentum and mass with the total velocity vector $\mathbf{U}(x, y, t) = (u(x, y, t), v(x, y, t) + V(x))$. We will assume that the edge wave velocity components u and v are small, u, $v \ll V$. The depth h and the longshore current V are assumed to be slowly varying in x alone (mild slope assumption). Retaining only those terms that are linear in u, v, and η gives

$$u_t + Vu_y = -g\eta_x \tag{1}$$

$$v_t + uV_x + Vv_y = -g\eta_y \tag{2}$$

$$\eta_t + \nabla(\eta V + h\mathbf{U}) = 0 \tag{3}$$

Subscripts indicate partial differentiation, and ∇ is the horizontal gradient operator. The x axis is taken positive in the offshore direction, and h is positive downward from the mean water level. Taking the form $f(x, y, t) = \mathrm{Re}\,[f'(x)e^{i(\kappa y - \sigma t)}]$ for u, v, and η, and substituting in (1) to (3) yields

$$u'(x) = \frac{-g\eta_x}{(-\sigma + \kappa V)} \tag{4}$$

$$v'(x) = \frac{-g\kappa\eta + V_x u}{(-\sigma + \kappa V)} \tag{5}$$

$$\eta'(x) = \frac{(hu)_x - \kappa h v}{(-\sigma + \kappa V)} \tag{6}$$

where Re indicates the real portion, and the x dependencies on the right-hand sides of the equations are understood. Dropping the prime notation for the cross-shore varying components, these equations can be manipulated to give a second-order differential equation in terms of either η

$$\left[\frac{gh\eta_x}{(-\sigma + \kappa V)^2}\right]_x + \eta\left[1 - \frac{\kappa^2 gh}{(-\sigma + \kappa V)^2}\right] = 0 \tag{7}$$

or u,

$$\left[\frac{\gamma^2}{(1-\gamma^2)}\left[\frac{hu}{(-\sigma + \kappa V)}\right]_x\right]_x - \gamma^2\kappa^2\left[\frac{hu}{-\sigma + \kappa V}\right] = 0 \tag{8}$$

where

$$\gamma^2 = \frac{(-\sigma + \kappa V)^2}{\kappa^2 gh} \tag{9}$$

In the nondivergent case (as $\gamma^2 \to 0$), and allowing complex values of σ, equation (8) reduces to equation (8) of *Bowen and Holman* [1989] for shear waves under the rigid-lid assumption. For $V(x) = 0$, equation (7) reduces to the classical edge wave equation in the absence of a current (for instance, *Holman and Bowen* [1979])

$$\left[\frac{gh\eta_x}{\sigma^2}\right]_x + \eta\left[1 - \frac{\kappa^2 gh}{\sigma^2}\right] = 0 \tag{10}$$

Of particular interest is the observation that if we make the substitution in (7) of

$$h'(x) = \frac{h(x)}{[1 - (V(x)/c)]^2} \tag{11}$$

where $h'(x)$ is defined as the effective beach profile and $c = \sigma/\kappa$ is the edge wave celerity (and carries the sign of κ), we get the result

$$\left[\frac{gh'\eta_x}{\sigma^2}\right]_x + \eta\left[1 - \frac{\kappa^2 gh'}{\sigma^2}\right] = 0 \tag{12}$$

which is functionally identical to the classical edge wave equation (10). The concept of the effective beach profile, $h'(x)$, is very useful in gaining a conceptual understanding of the combined role of the current and topography in modifying edge wave characteristics. Note that as $c \to V$, the

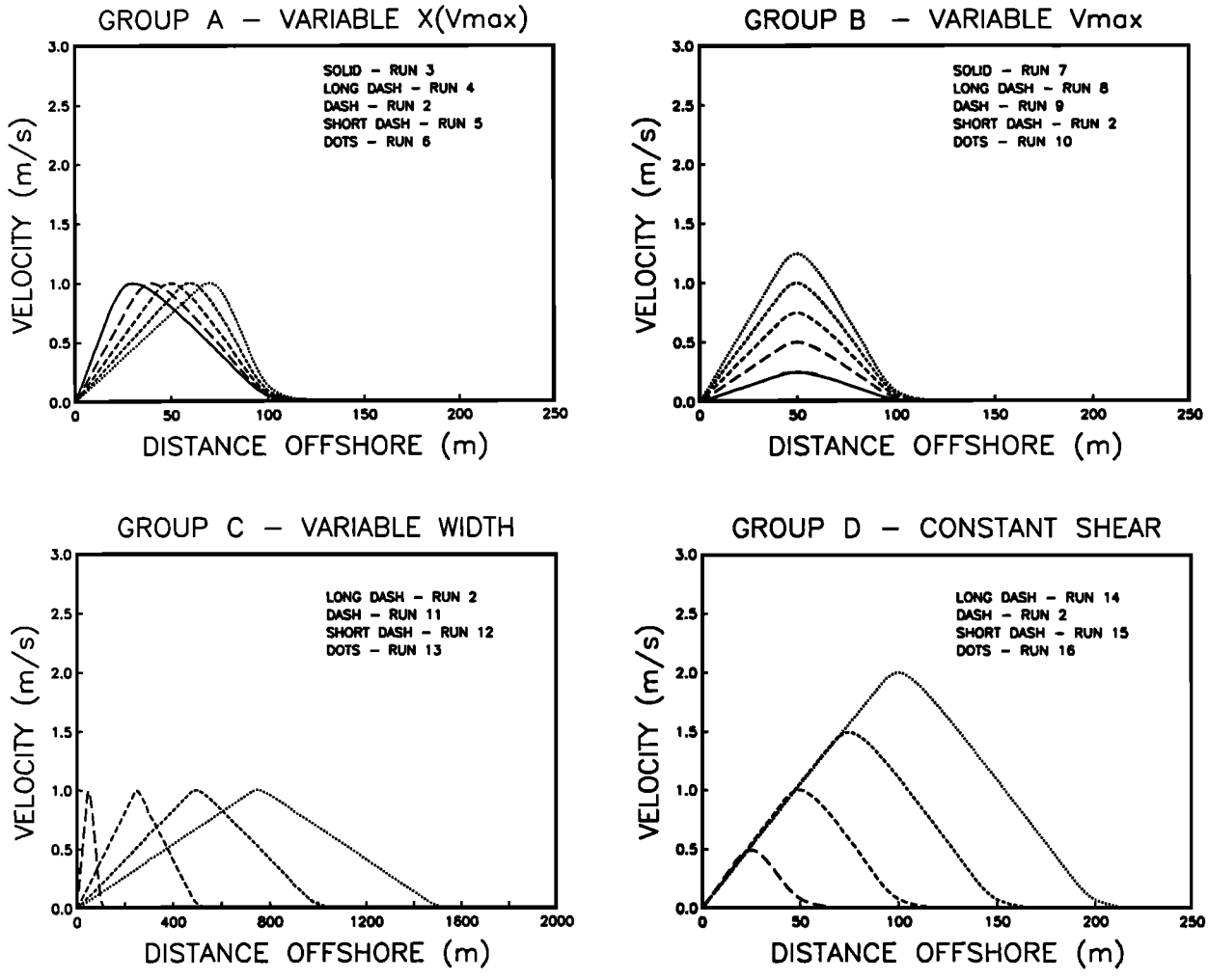

Fig. 2. Current profiles used for the test cases. The 16 runs have been broken into 4 groups. Group A holds V_{max} and x_w constant while varying $x(V_{max})$. Group B varies V_{max}, holding the width and $x(V_{max})$ constant. Group C holds V_{max} and the ratio of $x(V_{max})/x_w$ constant but varies the width and location of the maximum. Group D holds the landward face of the current to a constant shear but varies all three of the current parameters. Note the cross-shore scale is different for the group C plot.

effective depth approaches infinity and shallow water edge wave solutions are not valid.

Normal mode (edge wave) solutions are obtained by expressing (7) as two coupled first-order differential equations subject to the boundary conditions that $\eta(0)$ = finite and $\eta(\infty) = 0$. The coupled equations can be solved using a Runge-Kutta technique [*Press et al.*, 1986] starting from initial conditions at the shoreline. These are found by expanding h, V, and η in the form

$$h(x) = \beta_1 x + \beta_2 x^2 + \cdots \tag{13}$$

$$V(x) = \vartheta_1 x + \vartheta_2 x^2 + \cdots \tag{14}$$

$$\eta(x) = \eta_0(1 + \alpha_1 x + \alpha_2 x^2 + \cdots) \tag{15}$$

Substituting in (7) and equating terms of like powers of x gives

$$\eta(0) = \eta_0 = \text{given} \tag{16}$$

$$\eta_x(0) = \frac{-\sigma^2}{g\beta_1}\eta_0 = \alpha_1\eta_0 \tag{17}$$

$$\eta_{xx}(0) = \eta_0\left[\frac{1}{2}\left(\left(\frac{\sigma^2}{g\beta_1}\right)^2 + \kappa\right) + \frac{\sigma^2}{g\beta_1}\frac{\beta_2}{\beta_1} + \frac{2\kappa\vartheta_1\sigma}{g\beta_1}\right] = \alpha_2\eta_0 \tag{18}$$

These are identical to those found by *Holman and Bowen* [1979] with the exception of the ϑ_1 term in (18) expressing the added role of the longshore current shear.

As *Holman and Bowen* [1979] report, for any σ, κ pair the trial solution diverges from the boundary condition that $\eta \to 0$ at large x. The values of κ (holding σ constant) for which x is a local maximum before the solution diverges represent the set of edge wave modes which satisfy the edge wave dispersion relation (solve (7)) to the desired resolution. The solution method gives $u(x)$ and $\eta(x)$, while $v(x)$ is calculated from (5).

The results of the numerical scheme were tested against the two known analytical solutions for plane and exponential beaches, and against the approximation of *Kenyon* [1972] for very small currents. The dispersion relationship and other edge wave characteristics, such as nodal locations, were reproduced to arbitrary accuracy for the analytic cases, and Kenyon's approximation was found to be valid subject to his

stated constraints. The following results satisfy the dispersion relationship to ±0.1% in κ.

RESULTS

A total of 16 test cases were run in order to explore the sensitivity of edge waves to current magnitude and shape. Current profiles were constructed from two regions of constant shear, with the shear discontinuities smoothed using a 10-m-wide moving average. Three parameters were used to describe the current: the maximum current V_{max}, the cross-shore location of the maximum current, $x(V_{max})$, and the width of the current, x_w. Figure 2 summarizes the different current profiles used in this study. Much of the discussion is based on an example case, run 2 (which is common to the four groupings in Figure 2), with $V_{max} = 1.00$ m s^{-1} at $x = 50$ m with a width of ~100 m. For each current profile, solutions for modes 0–4 were determined at steps of 0.025 Hz from 0.2 to 0.05 Hz and at steps of 0.0025 Hz from 0.05 to 0.005 Hz.

All simulation runs used the same plane beach profile, $\beta = 0.035$, in order to facilitate comparison and more easily determine the current effects. The shallow water approximation for edge wave dispersion on a plane beach is given by *Eckart* [1951] as

$$\sigma^2 = g|\kappa|(2n + 1)\beta \tag{19}$$

where n is the edge wave mode number. Following *Holman and Bowen* [1979] and *Oltman-Shay and Guza* [1987], an effective beach slope felt by the edge waves in the presence of a longshore current, β_{eff}, can be defined as

$$\beta_{eff} \equiv \frac{\sigma^2}{g|\kappa|(2n + 1)} \tag{20}$$

allowing qualitative generalizations to be made regarding relative changes between the beach slopes (true and effective) and edge wave characteristics as we introduce different longshore current profiles (changing the effective beach profile).

Effects on Dispersion

Two general predictions can be made about the longshore current effects on edge wave dispersion. First, we expect the response to be asymmetric with regard to the direction of edge wave progression, and second, the maximum effect should occur at an intermediate value of frequency, decreasing for both high and low frequencies. The frequency dependence is related to the cross-shore scales of the edge wave and the current. For high frequencies (high wavenumbers), the edge wave is held tightly to shore and is not expected to be advected by the maximum current. For low frequencies, the edge wave extends well beyond the range of the current and experiences only a small perturbation. The effective beach profile (equation (11)) provides a convenient way to address the changes to dispersion (Figure 3). Edge waves progressing into the current ($V/c < 0$) have an effective profile which is shallower than the true profile, $\beta_{eff} < \beta$, thus $|\kappa|$ should increase. The opposite holds for those waves progressing with the current; the effective profile is deeper, resulting in an expected decrease in $|\kappa|$. We also expect the effects to increase as V increases (which in turn increases the departure of the effective profile from the true profile) as *Oltman-Shay and Guza* [1987] noted.

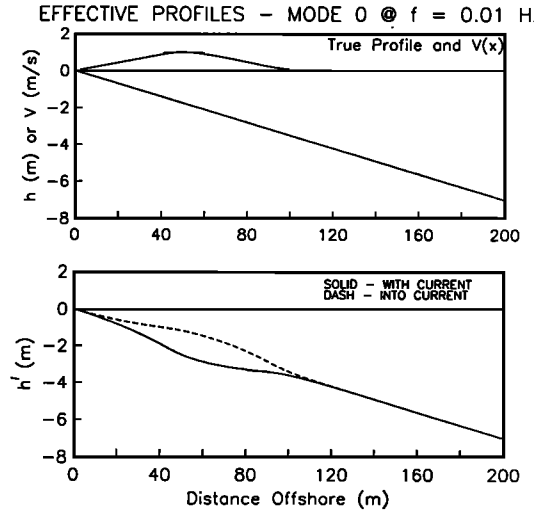

Fig. 3. The effective beach profiles for 0.010-Hz mode 0 edge waves for current run 2: (top) the true beach profile and the current; (bottom) plot of $h'(x)$. The resemblance of the profiles to either a terrace or a bar and trough is unmistakable. The solid line indicates the effective profile for edge waves progressing with the current; the dashed line indicates that for edge waves progressing into the current.

Figure 4 is a plot of the fractional wavenumber shift K for mode 0 edge waves as a function of frequency for all cases. We define K as

$$K = (\kappa - \kappa_p)/\kappa_p \tag{21}$$

with κ being the wavenumber in the presence of the current and κ_p being the wavenumber on the beach in the absence of a current (from (19)). Throughout these synthetic tests the signs of κ and κ_p are negative for edge waves progressing in opposition to the current. Edge waves progressing into the current are slowed so that $|\kappa|$ becomes larger (resulting in a positive value for K). Those edge waves progressing in the direction of the current propagate faster and $|\kappa|$ becomes smaller (giving a negative K).

Several of the expectations are verified. First, at both high and low frequencies the modification of the dispersion relation is generally small, with the maximum change (of up to 80% for these currents) occurring at an intermediate frequency. Second, the maximum $|K|$ for edge waves progressing into the current is greater, and the frequency at which it occurs is lower. Third, the magnitude of the change is a function of $x(V_{max})$ (Figure 4*a*), as well as the magnitude of V_{max} (Figure 4*b*).

The changes with increasing mode are clarified in Figure 5. The maximum value of K shifts to higher frequency as the mode increases. The magnitude of the effect on the mode 0 edge wave is greater than for the other modes, for which the maximum effects are roughly equal. The sensitivity of K to the match between the cross-shore scales of the edge wave and the current by plotting it versus $|k|x(V_{max})$ (Figure 6). We again see that an interior maximum occurs. For large $|k|x(V_{max})$, the effective profile on which the energetic portion of the edge wave exists does not depart greatly from the true profile. Similarly, for the lowest frequencies, the increase in edge wave celerity (as $|\kappa|$ decreases) acts to

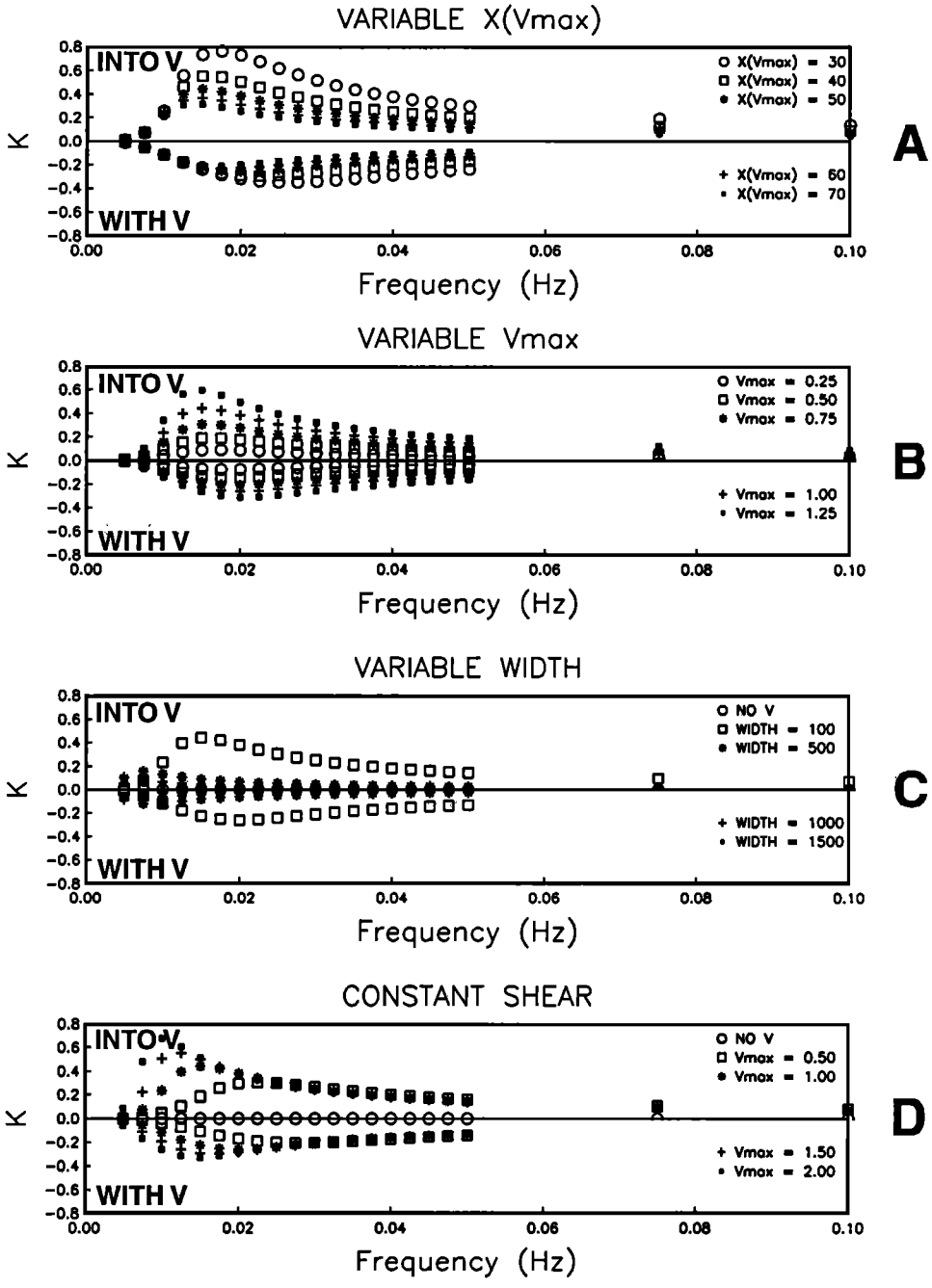

Fig. 4. The effect on dispersion, K, for each current group, as a function of frequency for the mode 0 edge waves (subject to $V_{max}/c < 1.$). Figures 4*a* to 4*d* refer to current groups A–D. In all cases except current run 13, the maximum effect is at an interior frequency. Note that the largest effect, near 80%, is for the current with the greatest shear on its landward face, corresponding to run 3.

decrease the magnitude of the ratio (V/c) and thus the departure of $h'(x)$ from the true profile. Restated, the energetic portion of the edge wave extends well beyond the width of the current, minimizing its effect. *Holman and Bowen* [1979] found a similar relationship between their effective beach slope, edge wave dispersion, and the beach morphology.

Effects on Cross-Shore Structure

The cross-shore dependence of an edge wave on a plane beach in the absence of a current, given by *Eckart* [1951], is

$$\phi(x) = A_n e^{-|\kappa|x} L_n(2|\kappa|x) \tag{22}$$

for $\eta(x)$ and $\nu(x)$, while $u(x)$ varies as ϕ_x, where A_n is the shoreline value, L_n is the Laguerre polynomial of order n, and n is the mode number. The cross-shore scale of the edge wave is clearly a function of $|\kappa|$; as $|\kappa|$ increases, the cross-shore scale decreases. As is seen by comparing the different directions of propagation in Figure 7, the nodal locations are modified as expected; as $|\kappa|$ increases for the edge waves progressing into the current the nodal structure moves closer to shore.

It is also instructive to compare the cross-shore structure

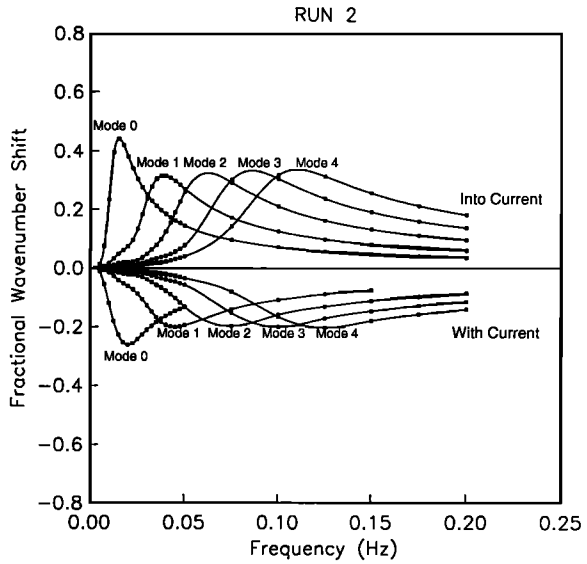

Fig. 5. The effect on dispersion for modes 0–4 for current run 2. The maximum effects are felt by the mode 0 edge waves. There is a clear increase in the frequency at which the maximum occurs as the mode number increases, suggesting a relationship between the cross-shore extent of the edge wave and the magnitude of the current effect.

in the presence of a current with that found on the plane beach of slope, β_{eff}, which results in the same σ-κ relationship (equation (20)). A sample comparison is shown in Figure 8. In this case, the nodes for all three profiles (u, ν, and η) are shifted landward of their locations on the equivalent plane beach. Figure 8 also illustrates that the amplitudes of the antinodes are also modified by the presence of a current, analogous to the changes reported by *Holman and Bowen* [1979] and *Kirby et al.* [1981] caused by nonplanar topography.

The impact of the current on the shape of $\nu(x)$ can be larger than on u or η. Equation (5) shows that $\nu(x)$ includes an advective term, uV_x. This term is important, particularly for the lower frequencies, where u remains relatively large at locations of sign changes in V_x. The spatial structure of the $\nu(x)$ profile is shown in Figure 9 for the first three modes at $f = 0.01$ Hz. The regions of large shear in the $\nu(x)$ profiles correspond with locations where the longshore current shear V_x changes sign ($x = 50$ m), and decreases to near zero ($x \sim 100$ m). Note that the variance profile $\nu^2(x)$ will be different for the two propagation directions and that in the case of the mode 1 edge wave, the uV_x contribution is actually great enough to introduce additional zero crossings into the $\nu(x)$ profile. The $+\kappa$ edge wave profile now has three crossings, while the $-\kappa$ edge wave has two. At the same cross-shore location, it is possible to be at a zero crossing for an edge wave progressing in one direction while near a maximum in variance for the edge wave progressing in the other direction. These additional zero crossings are not seen in the surface elevation profile, or in $u(x)$. The differences in the $\nu(x)$ variance between the two directions of edge waves, obvious from consideration of Figure 9, will be shown to be important for the correct interpretation of field data in the next section.

DISCUSSION

Implications for Field Data

The identification of low-mode edge waves has recently been shown to be possible using the longshore component of flow measured by alongshore arrays of bidirectional electromagnetic current meters deployed in the inner surf zone [*Huntley et al.*, 1981; *Oltman-Shay and Guza*, 1987]. Critical to the interpretation of these data has been correct prediction of edge wave dispersion, necessary for determination of the mode, as well as the cross-shore structure of the edge waves. These two pieces of information are needed to transform $\nu^2(\kappa, \sigma)$ measured at the array to the shoreline amplitude of the edge wave.

While the effects of longshore currents on edge wave dispersion have been dealt with in the past by common sense and assumption [*Oltman-Shay and Guza*, 1987; *Howd et al.*, 1991*a*], the effects on the cross-shore structure of the edge wave, particularly $\nu(x)$, have not been considered. A recent experiment, DELILAH, hosted by the Coastal Engineering Research Center (CERC) Field Research Facility (FRF) in Duck, North Carolina, during October 1990, provided an opportunity to test the impact of the improved theory.

The study beach is located on the Atlantic coast of the United States in the center of a 100-km-long barrier island. The primary source of data for this work was the inner array of current meters deployed in the surf zone, approximately 60 m from the mean shoreline in approximately 2-m water depth, where they remained submerged at all stages of the tide (Figure 10). Sensors were oriented such that $+V$ currents (alongshore) flow "south" parallel to the beach. The gages were wired to a computer-based collection system and were sampled at 8 Hz nearly continuously for a 3-week period. The FRF provided daily bathymetric surveys of the nearshore zone.

A 3-hour time period beginning at 1117 EST on October 11, 1990, and bracketing high tide has been selected to demonstrate the importance of the mean longshore current on edge wave properties. This period of time was characterized by a stable, linear sand bar, and a steady longshore current. The maximum mean (over the 3-hour period) longshore current was -108 cm s^{-1} (northward) in the trough of the bar, and decreased to -23 cm s^{-1} at the outermost current meter. The current was extrapolated beyond that point and cubic-spline interpolated between the instruments (Figure 11).

Alongshore wavenumber-frequency spectra were estimated using the iterative maximum likelihood estimator (IMLE) previously applied to surf zone data by *Oltman-Shay and Guza* [1987] and *Oltman-Shay et al.* [1989*b*]. The alongshore component of flow was used for the analysis, as it provides a natural filter to remove high mode and leaky wave variance as shown by *Oltman-Shay and Guza* [1987]. The first three edge wave modes were modeled for the true morphology and mean longshore current (Figure 12). Three topics will be discussed: the improvement in prediction of dispersion, prediction of the transition frequency between modes, and changes in the predictions of shoreline amplitudes.

The inclusion of the longshore current manifests itself in two ways: asymmetric wavenumber shifts (note the difference between the magnitudes of predicted plus and minus mode 0 wavenumbers at 0.05 Hz), and the compression of

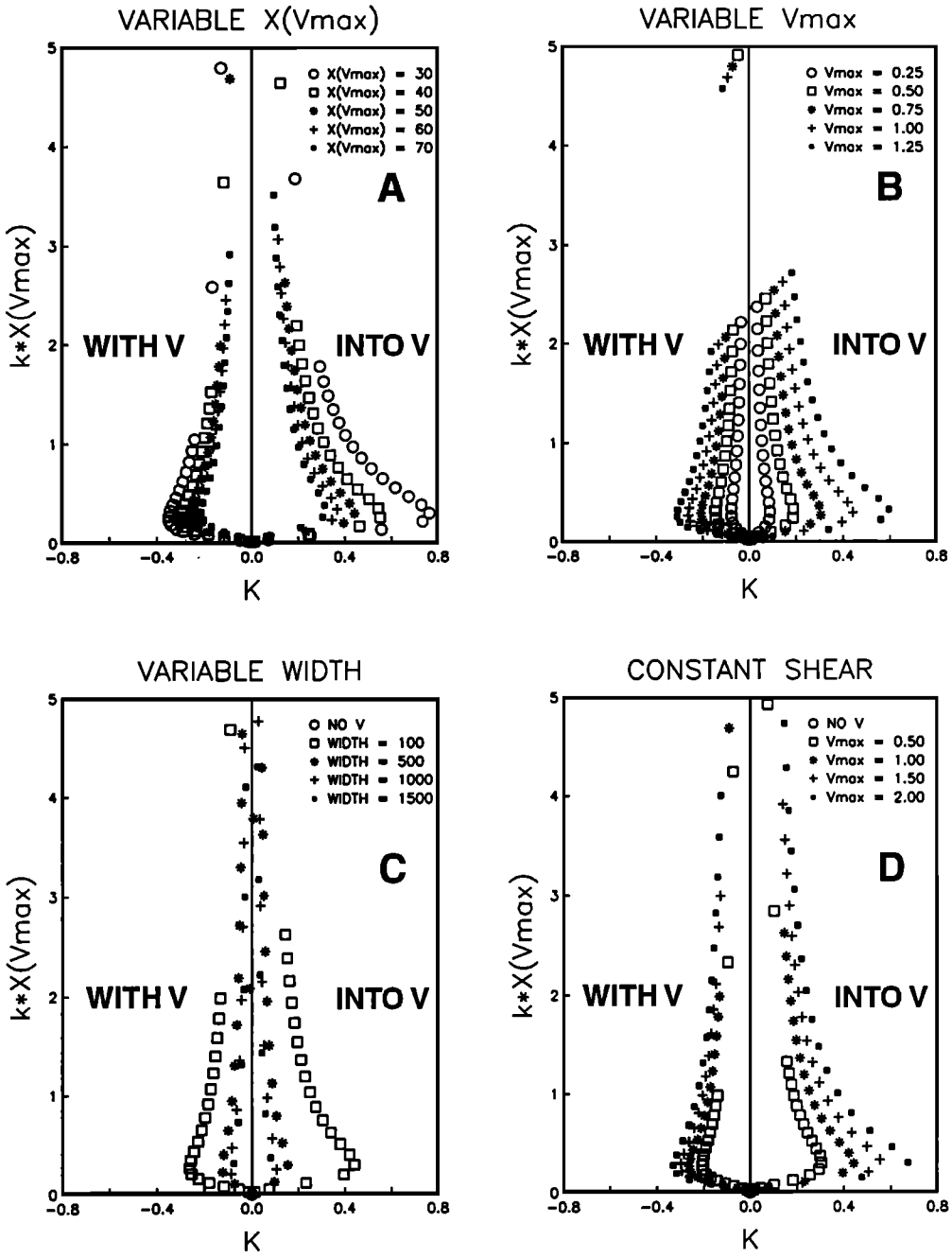

Fig. 6. K versus $|k|x(V_{max})$ for the mode 0 edge waves. Figures 6*a* to 6*d* refer to current group A–D.

dispersion lines with the current for the negative wavenumbers and the expansion of the dispersion curves for the edge waves progressing against the current for positive wavenumbers. The lower modes tend to be shifted more than the higher modes, be it an increase or decrease in $|\kappa|$. While this makes separation of modes difficult for the edge waves progressing with the current (negative wavenumbers in this case), it improves separation in the direction opposing the current.

K, the fractional wavenumber shift due to the current (equation (21)), is presented in Figure 13 as a function of frequency for the measured profiles. Many of the observations made with the synthetic tests hold here as well. The maximum effect (~30% for the edge waves opposing the current, ~20% for the edge waves progressing with the current) occurs at an intermediate frequency for mode 0. The maximum effect decreases in magnitude and shifts to higher frequencies for the higher modes. In contrast with the synthetic cases, the peak effect is felt over a much broader frequency range.

An excellent example of specific improvement in fitting modes to the data occurs for positive wavenumbers in the frequency range 0.02 to 0.04 Hz. This is shown in Figure 14. In the absence of the current (light arrows), the observed variance peaks fall between the predicted wavenumbers for the different modes. Inclusion of the current in prediction of the dispersion (dark arrows) greatly improves the correspondence between predicted and observed peaks. At 0.0405 Hz

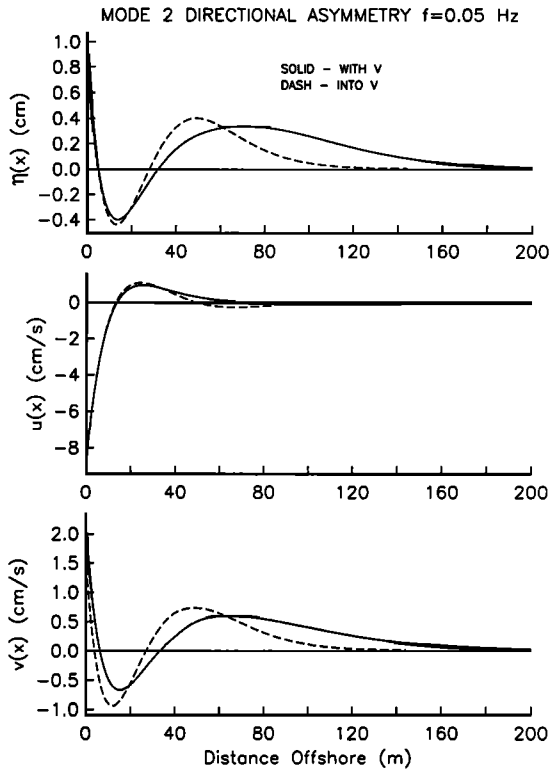

Fig. 7. Cross-shore profiles of (top) surface elevation, (middle) cross-shore velocity, and (bottom) longshore velocity for the mode 2 edge waves at 0.05 Hz for current run 2. The nodal locations are shifted landward and the antinodes are amplified for the edge waves progressing into the current. The phase of $v(x)$ into the current has been shifted by π to facilitate comparison.

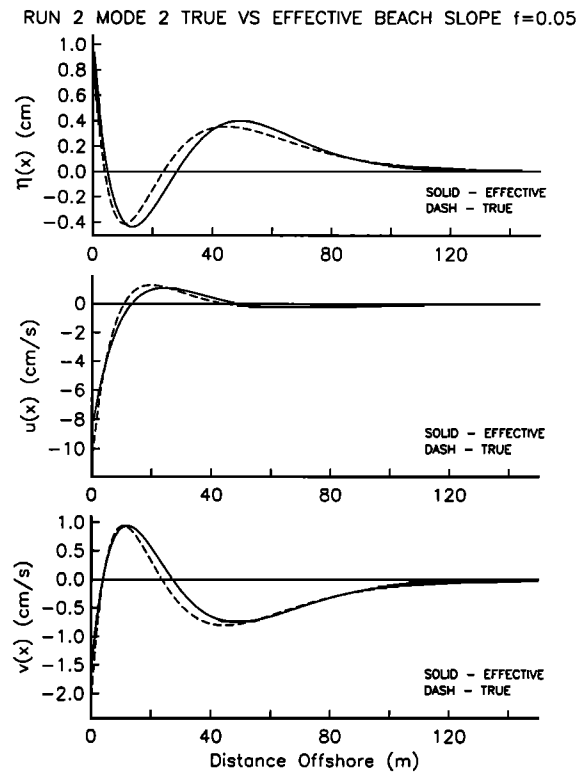

Fig. 8. A comparison between the cross-shore profiles of (top) η, (middle) u, and (bottom) v (the dashed lines) in the presence of a current (Run 2) with the solutions assuming a plane beach of slope β_{eff} (solid lines). Example shown is for the 0.05-Hz mode 2 edge wave progressing into the current. The shape of the edge wave is modified from that if the plane beach assumption had been made.

we see mode 1 edge waves progressing both directions, at 0.0308 Hz, mode 1 progressing south against the current, and at 0.0210 Hz, mode 0 edge waves again progressing both directions.

Close examination of the data presented in Figure 12 shows an important detail that is indicative of directional asymmetry. The mode 0 edge waves dominate the negative wavenumber edge waves up to a frequency of ~0.027 Hz where we begin to see evidence for mode 1 or 2 edge waves, while for the positive wavenumber edge waves, the transition from mode 0 to mode 1 occurs at a lower frequency, 0.023 Hz. These differences may have two causes, preferential forcing of certain modes, or the effects of the longshore current.

The modeled variance structure for mode 0–2 edge waves (all with shoreline amplitudes of 1 cm) as a function of frequency at the cross-shore location of the current meter array addresses these observations (Figure 15). In the absence of a longshore current, the frequency where the mode 0 variance drops below that of modes 1 and 2 would be the same for the two directions of edge wave propagation. The presence of the longshore current has caused shifts in the cross-shore shapes of the edge waves such that the mode 0–1 transition occurs at 0.0275 Hz for negative wavenumbers and at 0.0240 Hz for the positive wavenumbers. These frequencies closely correspond to the mode transitions seen in the data (Figure 12).

As an example of the effect of the longshore current on observed variance levels in the data, we will examine two frequency bands, those centered on 0.0210 Hz and 0.0405 Hz (Figure 14). The spectral peaks are associated with the mode 1 (0.0405 Hz) and mode 0 (0.0210 Hz) edge waves predicted by the model.

The observed ratio between the peak variances of the mode 0 edge waves ($-\kappa/+\kappa$) at 0.0210 Hz is 2.52; in the absence of a current we would expect the $-\kappa$ edge wave to have a similarly greater shoreline variance. However, the inclusion of the current effects in modeling $\nu^2(x)$ results in edge waves with identical shoreline elevations having a ratio between their variances of 1.92 at the array location (Figure 15). The ratio of these values indicates that the negative mode 0 edge wave should have larger shoreline variance by a factor of only 1.31 (2.52 ÷ 1.92) at the shoreline despite its much larger variance at the array location. Failure to include the effects of the longshore current would result in an overprediction by a factor of ~2 in the relative shoreline variances of these two waves.

A similar situation exists for the mode 1 edge waves at 0.040 Hz. The observed ratio of $-\kappa$ to $+\kappa$ peak variance is 1.90. Again, in the absence of a current, we would assume that this was a direct reflection of different shoreline variances. However, this is misleading, as model results predict a much smaller ratio of 0.45 at the array location for edge waves with equal shoreline amplitudes. In this case, the assumption of no current effect would lead to an underprediction of the relative shoreline variance by a factor of ~4.22.

The possibility of such strong asymmetry being introduced

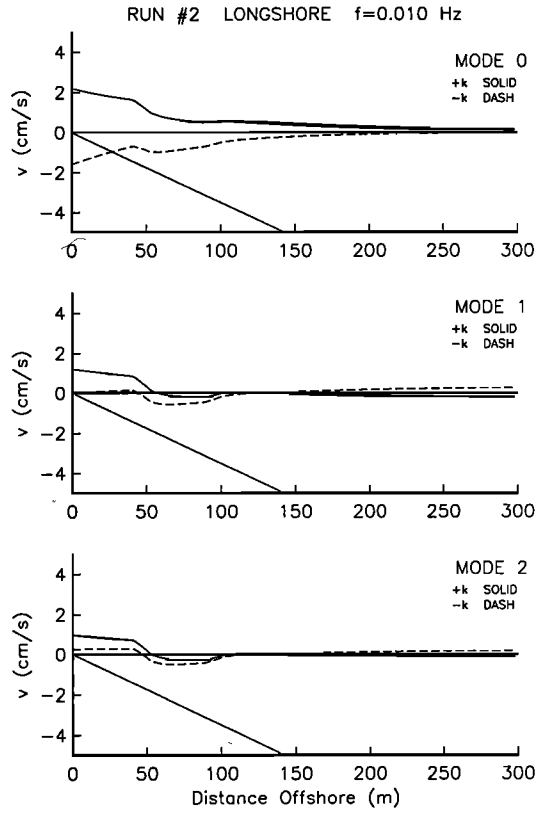

Fig. 9. Profiles of $v(x)$ for the first three modes at $f = 0.01$ Hz for current run 2. The "kinks" in the profiles are the result of the advective momentum term uV_x in equation (5) changing sign at $x = 50$, then going to 0 at $x \sim 100$. The effect is to increase the number of zero crossing in this component of flow and to significantly alter the variance structure (v^2) between edge waves progressing opposite directions. The profiles of η and u (not shown) do not have the additional zero crossings.

into the edge wave $v^2(x)$ profiles by the longshore current makes it important that the current be adequately measured and accounted for in data analysis if the shoreline amplitudes of the edge wave are required. This topic is discussed further by J. Oltman-Shay and P. A. Howd (The interpretation of infragravity edge wave field observation on beaches with nonplanar bathymetry and mean alongshore currents, submitted to *Journal of Geophysical Research*, 1991), in the context of a reexamination of edge wave amplitudes originally presented by *Oltman-Shay and Guza* [1987].

Modification of Topography

Perhaps the most obvious impact of the inclusion of the longshore current effects on models for the generation of topography due to edge waves is the modification of the dispersion relationship. Edge waves of the same mode and frequency progressing in opposite directions no longer have equal magnitude wavenumbers. Thus a crescentic sand bar system, predicted by *Bowen and Inman* [1971] for phase-locked edge waves of equal frequency and mode but opposite directions of progression could be stretched into the oblique welded bar predicted by *Holman and Bowen* [1982] for the case of two phase-locked edge waves of equal frequencies but different $|\kappa|$ of opposite sign.

A more interesting role in the evolution of topography is suggested by the shapes of the effective profiles. Recalling Figure 3, the effective profiles are very reminiscent of either bar and trough topography for the edge waves progressing with the current, or terrace topography for those opposing the current. The possibility of feedback from the effective topography (i.e., due to the longshore current structure) in the determination of the true topography will be briefly explored using one of the synthetic cases presented earlier; a test with field data is beyond the scope of this paper.

Following *Hunt and Johns* [1963] and *Holman and Bowen* [1982], the cross-shore drift velocity of a progressive edge wave at the top of the bottom boundary layer, $\hat{u}(x)$, can be expressed as

$$\hat{u}(x) = \frac{-1}{4\sigma}(3uu_x - \kappa uv) \tag{23}$$

and the x dependencies on the right-hand side are understood. We will examine the drift velocity defect, $\Delta\hat{u}(x)$, defined as

$$\Delta\hat{u}(x) = \hat{u}(x) - \hat{u}_p(x) \tag{24}$$

where $\hat{u}_p(x)$ is the drift velocity on a plane beach in the absence of a current.

If the existing profile results from the balance between gravity (always working downslope), the edge wave drift velocities, and the incident waves, we can conceptualize the changes which will result from the modification of the edge waves (due to the addition of a longshore current) in terms of the differential transport, which [after *Holman and Bowen*, 1982], should be of a form similar to

$$\Delta i_x = \frac{\varepsilon_s C_d \rho}{w}\frac{16}{15\pi}\left(5u_0^3\Delta\hat{u} + \frac{u_0^5}{w}\frac{d\hat{h}}{dx}\right) \tag{25}$$

where Δi_x is the differential suspended transport in the cross-shore direction, u_0 is a characteristic incident wave orbital velocity, ρ and w are the sediment density and fall velocity, ε_s and C_d are an efficiency and drag coefficient, respectively, and finally, $\hat{h}$ is the perturbation to the bed away from its old equilibrium position. The new equilibrium profile is defined by the condition $\Delta i_x = 0$ for all x, giving

$$\frac{d}{dx}\hat{h}(x) = \frac{-5w\Delta\hat{u}}{u_0^2} \tag{26}$$

Integrating from deep water toward the shoreline gives the perturbation profile. The u_0 profile is specified as by *Holman and Bowen* [1982] seaward of the break point (u_0 increases slowly to the break point). A depth-dependent breaking region with decreasing velocity has been added from the break point to the shoreline. Because u_0 goes to zero at the shoreline, the integration of (26) is invalid very close to shore. Readers interested in the details of this formulation are referred to *Holman and Bowen* [1982].

There are two primary contributions to $\Delta\hat{u}(x)$ (thus to the perturbation topography): the shift of the nodal structure as κ changes (due to the dispersion effects of the longshore current) and the "kinks" in the $v(x)$ profiles introduced by the longshore current shear (Figure 9; equation (5)). It is important to note that while the cross-shore location of the nodal structure will change (and with it the preferred location of the sand bar) with frequency and mode, perturbations

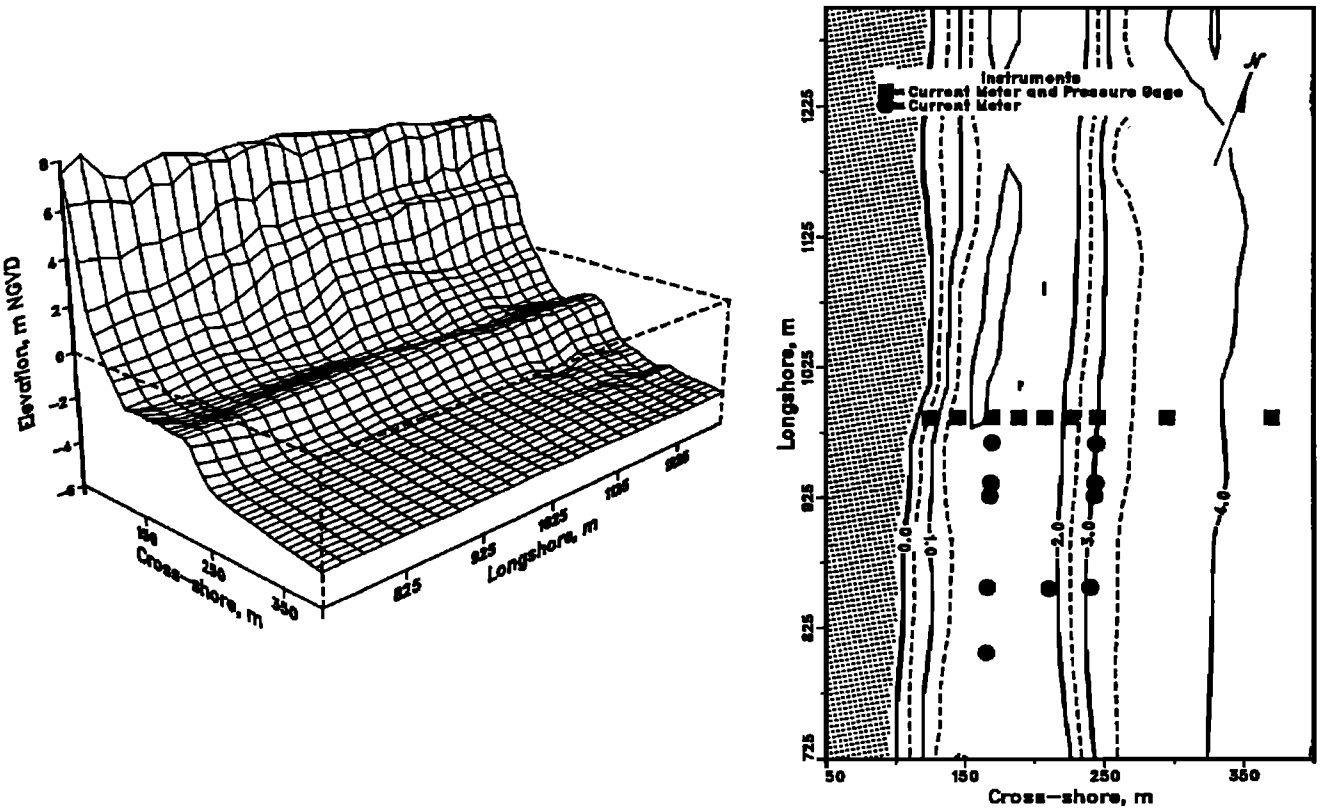

Fig. 10. Morphology and sensor locations for October 11, 1990, at the DELILAH experiment. The inner array of current meters was in the trough of the linear sand bar. The longshore current was to a great extent contained within the cross-shore scale of the array. Figure courtesy of B. Birkemeier, Chief, CERC Field Research Facility.

to $\nu(x)$ (and through (23) to $\hat{h}(x)$) resulting from the longshore current shear change only in magnitude and have a fixed cross-shore location (equation (5)). This should provide a consistent cross-shore scale for the perturbation topography (for one direction of edge wave progression) even in the presence of a broad-banded edge wave field (where the nodes are not at a constant cross-shore distance).

A test of the robust nature of this hypothesis is presented in Figure 16, which shows the result of adding the perturbation profiles for all the modeled edge waves, modes 0–4, with $\kappa > 0$, for the frequency range 0.05–0.005 Hz. The integrated perturbation profile for the edge waves progressing with the current shows the formation of a sand bar 100 m offshore, the same location predicted by the effective profile (Figure 3). Note that a result similar to the effective profile occurs for the case of edge waves opposing the current as well. In that case, the total perturbation profile is indicative of a terrace, much closer to the shoreline.

The perturbation profile results for edge waves going with and against the current are opposite; thus for one response to dominate, so must one direction of edge wave progression. It has been shown both theoretically [*Bowen and Guza*, 1978] and in field data [*Oltman-Shay and Guza*, 1987; *Oltman-Shay et al.*, 1989*a*] that under obliquely incident wave conditions, edge waves may be preferentially forced in the same direction as the forcing of the longshore current. Thus a bar-trough topography is expected. *Howd et al.* [1991*b*] present an initial look at field data showing the evolution of a linear bar during a storm and report that there are preliminary indications of the effective profile providing positive feedback to the evolution of the true profile.

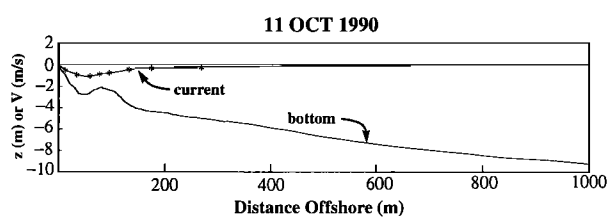

Fig. 11. Beach and longshore current profiles used to solve for edge wave characteristics on October 11, 1990.

While the details of the present "model" are admittedly simplistic, the results appear to be robust. Edge wave kinematics are clearly altered in a manner that scales with the longshore current geometry over a wide range of frequencies and wavenumbers. The longshore current effects on edge wave drift velocities may well provide a positive feedback mechanism, through the effective beach profile, for the evolution of the true profile. These results should be interpreted not as quantitative, rather as a qualitative prediction of the tendency for net sediment transport by edge waves perturbed by a longshore current. Obviously, the total transport of sediment in the surf zone is much more complicated than is allowed by the simple formulation presented here. Nevertheless, the prediction of a linear bar in the presence of a broad-banded edge wave field is an intriguing improvement upon previous models of linear bar formation by infragravity waves which have relied upon the assumption of a narrow-banded infragravity wave field.

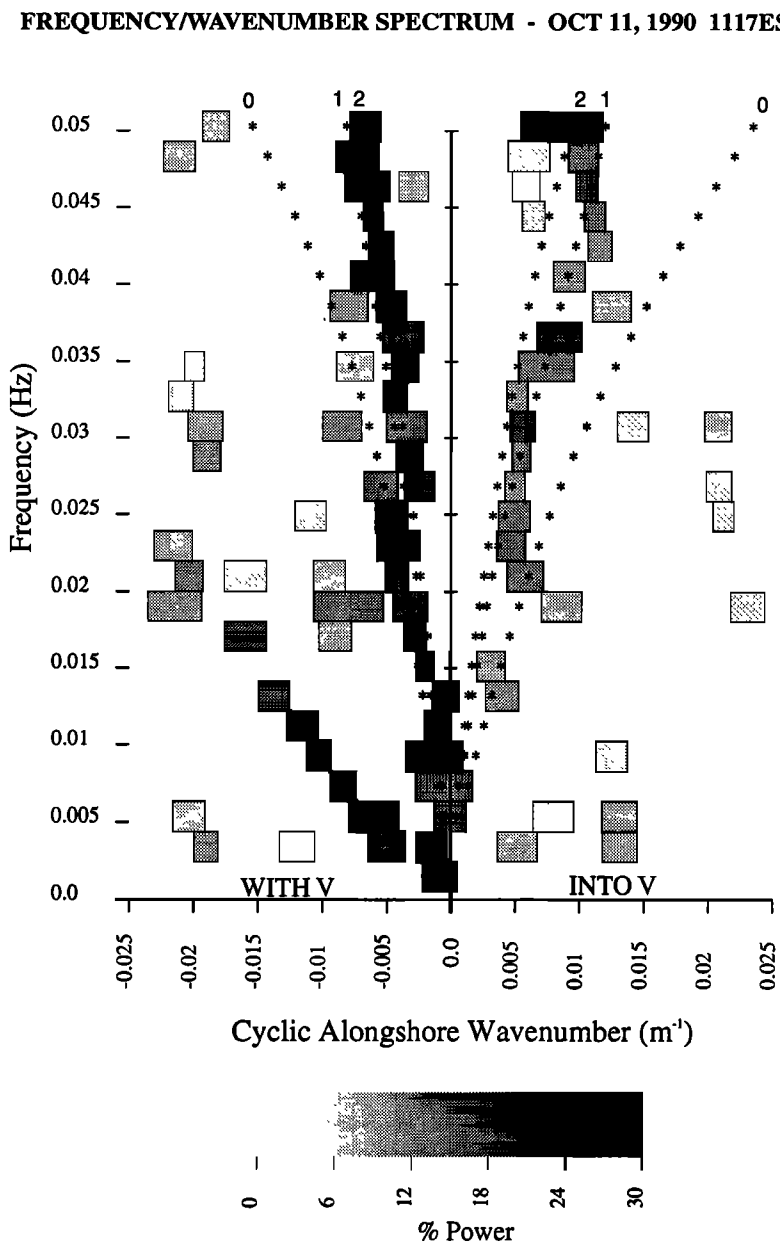

Fig. 12. Frequency-wavenumber spectrum from October 11, 1990. The horizontal axis is the cyclic wavenumber ($k = 1/L_y$); the vertical axis shows the frequency ($f = 1/T$). The shaded squares represent concentrations of variance in k-f space, with the darker boxes indicating a greater percent of that frequency band's energy. The height of the boxes is the frequency bandwidth; the width represents the half-power wavenumber bandwidth of the spectral peaks which exceed the noise floor. The numerical solutions for edge wave dispersion for the first three modes for each direction are indicated by the asterisks. The longshore current during this time flowed in the direction of negative wavenumbers (north).

CONCLUSIONS

We have shown that longshore currents modify refraction in the nearshore waveguide, changing the dynamics and kinematics of edge waves. A form of the linear, inviscid shallow water wave equation, which includes realistic longshore currents and bathymetry, was derived. This equation provides a continuum of solutions between gravity waves (either leaky or edge waves) and the recently discovered shear waves. For edge waves and leaky waves, the current effects can be uniquely accounted for in terms the effective beach profile, $h'(x) = h(x)\,[1 - (V(x)/c)]^{-2}$. The effective profile is particularly useful in conceptualizing the combined effects of longshore currents and variable bottom topography provided that $V_{max}/c < 1$.

Numerical solutions have shown the edge wave dispersion relationship and the cross-shore shapes of edge waves to be sensitive to the presence of a current. Changes to the edge wave alongshore wavenumber κ of up to 30% are found for field data. Unlike nonplanar topography, the longshore current introduces anisotropy into the edge wave dispersion relationship, with $|\kappa|$ increasing for edge waves opposing the current flow, and decreasing for those edge waves coincident with the flow. The cross-shore structure of the edge waves is also strongly modified. As expected, as $|\kappa|$ increases (de-

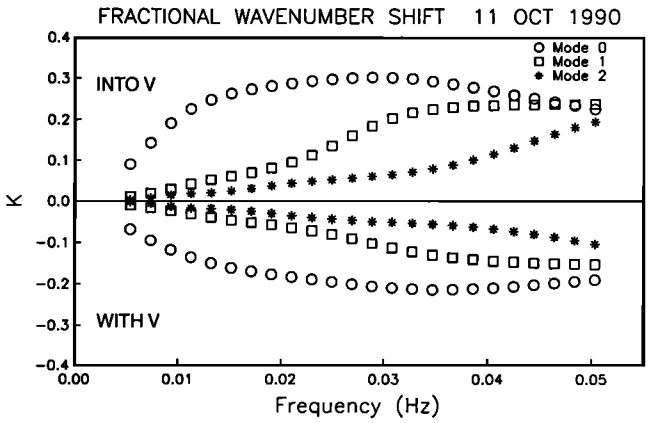

Fig. 13. K versus f for the measured profiles of $h(x)$ and $V(x)$ on October 11, 1990. The normalizing wavenumbers κ_p are from numerical solutions on the true morphology in the absence of a longshore current.

creases), the nodal structure shifts landward (seaward) from the positions in the absence of a current. In addition, the predicted variances away from the nodes, particularly for the alongshore component of edge wave orbital velocity, may change dramatically from the no-current case. Failure to account for these changes can lead to incorrect identification of modes and large differences in the estimation of the corresponding shoreline amplitude.

The magnitudes of many of the edge wave responses are

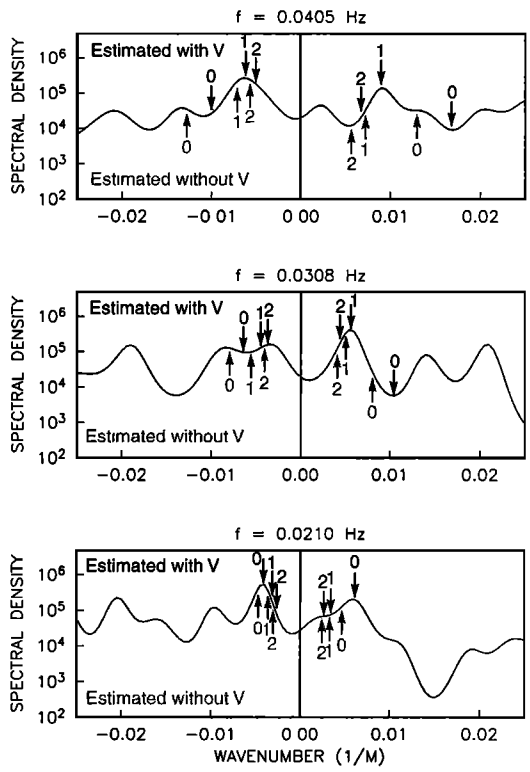

Fig. 14. Wavenumber spectra for three frequency bands, 0.0210 Hz, 0.0308 Hz, and 0.0405 Hz, for the data shown in Figure 12. Peaks in the observed wavenumber spectra correspond much better with the wavenumber predictions which include the effects of the longshore current (the black arrows pointing down from above the curves) than with the estimates which do not include current effects (gray arrows pointing up from below the curves).

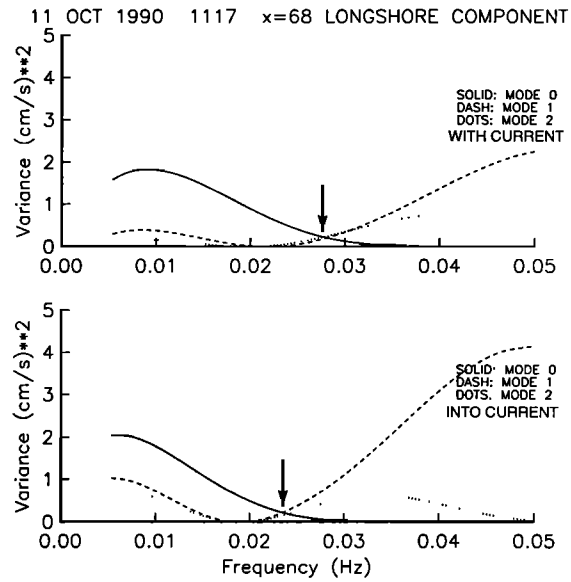

Fig. 15. Modeled variance of the longshore component of edge wave flow versus frequency for the first three modes at the cross-shore location of the array assuming equal shoreline amplitudes (1 cm) for all frequencies and modes. The frequencies where the mode 0 variance dips below that of the higher modes, indicated by the arrows, are also seen in the field data (Figure 12).

related to the ratio V_{max}/c, where V_{max} is the maximum current, and to the dimensionless cross-shore scale of the current, $|\kappa|x(V_{max})$, where $x(V_{max})$ is the cross-shore distance to V_{max}. This is most easily understood in terms of the effective profile and the strong dependence of the edge waves to the details of the inner part of the beach profile.

Examination of field data supports the importance of correct modeling of longshore current effects. Inclusion of the current was needed for correct identification of the different edge wave modes. For the case discussed, the longshore current (maximum mean velocity of -108 cm s^{-1}) produced shifts in the dispersion relationship in excess of 20% over much of the infragravity band. Differences of up to a factor of 4 in relative shoreline variance for edge waves of the same mode and frequency, but progressing in opposite directions, were shown to be possible between solutions which did and did not account for the longshore current.

Inclusion of longshore current effects may also have strong implications regarding the role of edge waves in the generation of nearshore morphology. The most obvious of these is the result of changes to the dispersion relationship. In the absence of a current, up and down coast edge waves of equal frequency and mode have the same $|\kappa|$. If the waves are phase locked, a crescentic bar is expected to result [*Bowen and Inman*, 1971]. However, in the presence of a current, the $|\kappa|$ magnitudes differ and presumably a more complicated pattern would result, perhaps resembling the welded bar result of *Holman and Bowen* [1982].

The most interesting effect is the positive feedback between the effective topography and the true profile. The cross-shore component of the edge wave drift velocity is modified in such a way that the effective topography is enhanced in the true profile. The perturbation profile results from two effects, the shifting of the nodal structure as the current changes the dispersion relationship, and the importance of the longshore current shear on the $\nu(x)$ profile of the

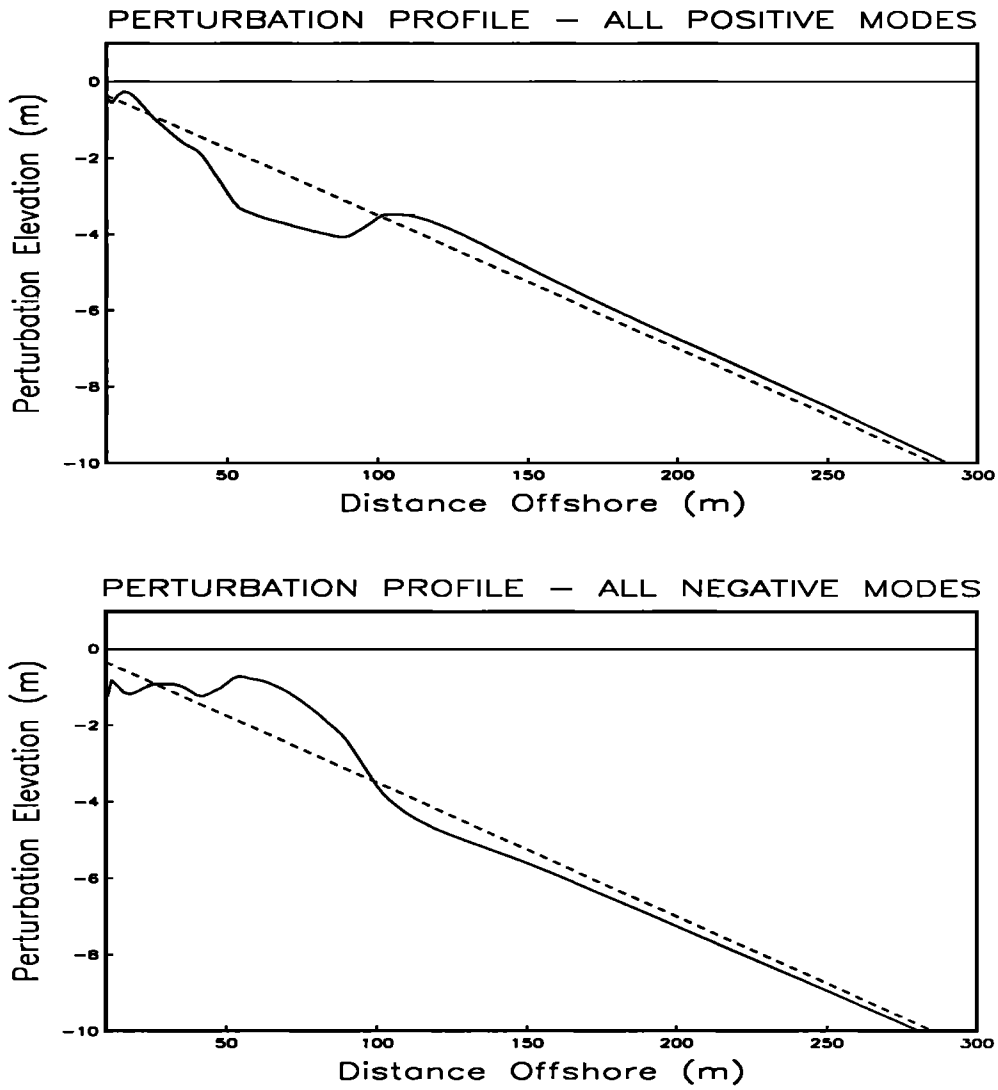

Fig. 16. Total profiles ($h + \hat{h}$) for edge waves with f less than or equal to 0.05 Hz modeled in run 2 (modes 0 to 4) progressing (top) with the current and (bottom) against the current. Topographies (bar and trough or terrace) with the same cross-shore scale as the effective profile (Figure 3) are predicted.

edge wave. Because the longshore current profile is assumed fixed in time and space, it provides a consistent perturbation regardless of edge wave frequency or mode. This is attractive because it provides an independent cross-shore scale for edge wave generation of sand bars, requiring only that one direction of progression be dominant.

Acknowledgments. This research was funded by the National Science Foundation (grant OCE87-11121) and the Office of Naval Research, Coastal Sciences Program (grant N00014-90-J-1118). The field data collection was funded by the Coastal Engineering Research Center, the Office of Naval Research, and, for profiling support, the U.S. Geological Survey. The surf zone instrument arrays comprised sensors belonging to Ed Thornton, Naval Postgraduate School, and Bob Guza, Scripps Institution of Oceanography. Their generosity with the data is greatly appreciated. Frequency-wavenumber analyses of the field data were accomplished using programs written by Joan Oltman-Shay, Quest Integrated. Bob Guza is also thanked for his comments and the clarity they provided during preparation of this paper. Thanks are also extended to the guys in the lab back in Corvallis and to John Haines and Jeff List. Their comments on one draft or another helped this paper along. Support for preparation of the final draft and publication of this paper came from the U.S. Geological Survey, Geologic Division Postdoctoral Program, through Research Opportunity 90-A-2.

REFERENCES

Ball, F. K., Edge waves in an ocean of finite depth, *Deep Sea Res.*, *14*, 79–88, 1967.

Bowen, A. J., Simple models of nearshore sedimentation; Beach profiles and longshore bars, in Coastline of Canada, *Geol. Surv. Pap. Geol. Surv. Can.*, *80-10*, 21–30, 1981.

Bowen, A. J., and R. T. Guza, Edge waves and surf beat, *J. Geophys. Res.*, *83*, 1913–1920, 1978.

Bowen, A. J., and R. A. Holman, Shear instabilities of the mean longshore current, 1, Theory, *J. Geophys. Res.*, *94*, 18,023–18,030, 1989.

Bowen, A. J., and D. L. Inman, Rip currents, 2, Laboratory and field observations, *J. Geophys. Res.*, *74*, 5479–5490, 1969.

Bowen, A. J., and D. L. Inman, Edge waves and crescentic bars, *J. Geophys. Res.*, *76*, 8662–8671, 1971.

Eckart, C., Surface waves on water of variable depth, *Wave Rep. 100, Ref. 51-12*, 99 pp., Scripps Inst. of Oceanogr., Univ. of Calif., La Jolla, 1951.

Elgar, S., and R. T. Guza, Observations of bispectra of shoaling surface gravity waves, *J. Fluid Mech.*, *161*, 425–448, 1985.

Gallagher, B., Generation of surf beat by non-linear wave interactions, *J. Fluid Mech.*, *49*, 1–20, 1971.

Guza, R. T., and D. L. Inman, Edge waves and beach cusps, *J. Geophys. Res.*, *80*, 2997–3012, 1975.

Guza, R. T., and E. B. Thornton, Swash oscillations on a natural beach, *J. Geophys. Res.*, *87*, 483–491, 1982.

Guza, R. T., and E. B. Thornton, Observations of surf beat, *J. Geophys. Res.*, *90*, 3161–3172, 1985.

Holman, R. A., Infragravity wave energy in the surf zone, *J. Geophys. Res.*, *86*, 6422–6450, 1981.

Holman, R. A., and A. J. Bowen, Edge waves on complex beach profiles, *J. Geophys. Res.*, *84*, 6339–6346, 1979.

Holman, R. A., and A. J. Bowen, Bars, bumps, and holes: Models for the generation of complex beach topography, *J. Geophys. Res.*, *87*, 457–468, 1982.

Holman, R. A., and A. J. Bowen, Longshore structure of infragravity wave motions, *J. Geophys. Res.*, *89*, 6446–6452, 1984.

Holman, R. A., and A. H. Sallenger, Setup and swash on a natural beach, *J. Geophys. Res.*, *90*, 945–953, 1985.

Howd, P. A., J. Oltman-Shay, and R. A. Holman, Wave variance partitioning in the trough of a barred beach, *J. Geophys. Res.*, *96*, 12,781–12,795, 1991*a*.

Howd, P. A., A. J. Bowen, R. A. Holman, and J. Oltman-Shay, Infragravity waves, longshore currents and linear sand bar formation, in *Proceedings, Coastal Sediments '91*, p. 72–84, American Society of Civil Engineers, New York, 1991*b*.

Hunt, J. N., and B. Johns, Current induced by tides and gravity waves, *Tellus*, *15*, 343–351, 1963.

Huntley, D. A., R. T. Guza, and E. B. Thornton, Field observations of surf beat, 1, Progressive edge waves, *J. Geophys. Res.*, *86*, 6451–6466, 1981.

Kenyon, K. E., Wave refraction in ocean currents, *Deep Sea Res.*, *18*, 1023–1034, 1971.

Kenyon, K. E., Edge waves with current shear, *J. Geophys. Res.*, *77*, 6599–6603, 1972.

Kirby, J. T., R. A. Dalrymple, and P. L.-F. Liu, Modification of edge waves by barred beach topography, *Coastal Eng.*, *5*, 35–49, 1981.

Lippmann, T. C., and R. A. Holman, The spatial and temporal variability of sand bar morphology, *J. Geophys. Res.*, *95*, 11,575–11,590, 1990.

Oltman-Shay, J., and R. T. Guza, Infragravity edge wave observations on two California beaches, *J. Phys. Oceanogr.*, *17*, 644–663, 1987.

Oltman-Shay, J., S. Elgar, and P. Howd, Observations of infragravity-frequency long waves, II. Comparisons with a 2-D wave group generation model (abstract), *Eos Trans. AGU*, *70*, 1333, 1989*a*.

Oltman-Shay, J., P. A. Howd, and W. A. Birkemeier, Shear instabilities of the mean longshore current, 2, Field data, *J. Geophys. Res.*, *94*, 18,031–18,042, 1989*b*.

Press, W. H., B. P. Flannery, S. A. Teukolsky, and W. T. Vetterling, *Numerical Recipes: The Art of Scientific Computing*, Cambridge University Press, New York, 1986.

Sallenger, A. H., R. A. Holman, and W. A. Birkemeier, Storm-induced response of a nearshore-bar system, *Mar. Geol.*, *64*, 237–257, 1985.

Short, A. D., Multiple offshore bars and standing waves, *J. Geophys. Res.*, *80*, 3838–3840, 1975.

A. J. Bowen, Department of Oceanography, Dalhousie University, Halifax, Nova Scotia, Canada B3H 4J1.

R. A. Holman, College of Oceanography, OC Administration Building 104, Oregon State University, Corvallis, OR 97331.

P. A. Howd, Center for Coastal Geology, U.S. Geological Survey, 600 Fourth Street South, St. Petersburg, FL 33701.

(Received July 23, 1991;
accepted January 23, 1992.)